

Reliable 3D Surface Acquisition, Registration and Validation using Statistical Error Models

J. Gühring

Institute for Photogrammetry, University of Stuttgart
Geschwister-Scholl-Str. 24D, D-70174 Stuttgart, Germany
Email: Jens.Guehring@ifp.uni-stuttgart.de

Abstract

We present a complete data acquisition and processing chain for the reliable inspection of industrial parts considering anisotropic noise. Data acquisition is performed with a stripe projection system that was modelled and calibrated using photogrammetric techniques. Covariance matrices are attached individually to points during 3D coordinate computation. Different datasets are registered using a new multi-view registration technique. In the validation step, the registered datasets are compared with the CAD model to verify that the measured part meets its specification. While previous methods have only considered the geometrical discrepancies between the sensed part and its CAD model, we also consider statistical information to decide whether the differences are significant.

1 Introduction

Coordinate measuring machines are the defacto standard for industrial part inspection, but suffer from limitations such as high cost and low measurement speed [7]. On the other hand, optical 3D shape acquisition systems provide fast and dense surface measurements without the need for physically probing surfaces, thus making them ideally suited for various applications in industrial inspection and reverse engineering. However, industry acceptance does not adequately reflect the theoretical and practical performance of these systems. One reason for the slow industry acceptance is the absence of standards, as they exist for coordinate measurement machines on a national and international level [19]. To fill this gap, some national standard organizations are now working on similar standards for optical measurement systems [30]. Another reason is measurement uncertainty, which is not constant over the measurement volume. It rather depends on a number of factors like sensor hardware, sensing geometry and the shape and reflectance properties of the object under

consideration. Inspection results usually require a number of further processing steps. Thus, the achieved accuracy is hard to estimate, even for experienced operators.

In this paper, we present a complete processing chain for industrial part inspection that provides the user not only with the geometric difference between the measured object and its CAD model, but also with the uncertainty in the obtained results. Data acquisition is performed using a commercial stripe projection system. We replaced the manufacturers software by our own calibration and processing methods, which are based on photogrammetric techniques. This allows us to quantify measurement uncertainty, characterized by an error covariance matrix and propagate it through all processing steps. Covariance information is also used to improve registration accuracy within pairwise registration and within a new multi-view registration procedure. The geometric deviation between the sensed surface and the CAD model is computed in the validation step. Statistical tests can then be applied to convert the validation results into a traffic light model where red stands for a significant discrepancy, yellow indicates potential problems and green indicates that the part or a specific feature meets its specification. Therefore, the user can easily judge the results in a transparent manner.

The remainder of this section presents a short survey of previous work on the related topics. Section 2 covers calibration and data acquisition issues. Section 3 describes new methods in view registration. Section 4 concludes the paper and discusses the obtained results.

1.1 Previous Work

A number of different sensor architectures have been proposed for the construction of range sensors. Comprehensive reviews can be found in [3] and [14]. Active triangulation is one of the most common methods for 3D surface acquisition. Such systems project specific light patterns onto the object. The light patterns are distorted by the object surface and observed by at least one camera. The distorted patterns can then be used to

efficiently reconstruct the objects surface. The systems differ primarily in the type of illumination (laser or incoherent light source) and the dimensionality of the camera (matrix or linear array) and the pattern (dot, stripe, multi dot/stripe or freely programmable, e.g. LCD projector) [23,35].

More recently, authors made an effort to improve aspects like calibration, accuracy and reliability. [10] consider the time evolution of the reflected pattern while sweeping a laser plane over the object. Their so-called spacetime analysis considerably reduces a number of error sources in traditional methods if surface discontinuities and changes in surface reflectance are present. Trucco et al [26] addressed the issues of calibration, stripe location and measurement consistency. They proposed several explicit consistency tests based on two-camera geometry.

Calibration is usually performed using one of two basic approaches. Direct calibration uses an arbitrary calibration function (usually a polynomial) to describe the mapping from observations to three-dimensional coordinates. The parameters of this function are obtained by measuring a large number of well-known points throughout the measuring volume. An immediate advantage is, that no care has to be taken to model any phenomena, since every source of error is implicitly handled by the computed coefficients [26]. However, direct calibration requires a highly accurate calibration normal. Especially for sensors with a large measurement volume, this requirement complicates the calibration procedure or makes it even impossible. Since the calibration function acts as a black box, there is no information about the quality of measurements.

In model-based calibration, parameters of a geometric model of the sensor, so called intrinsic and extrinsic parameters, are determined. The model describes how points in 3D space are projected onto the image plane, considering imperfect cameras and lenses. Most commonly a specially designed test object is used to effectively compute the desired quantities from a few calibration measurements [8,15]. Since any short-term geometrically stable object can be used for calibration, there is no need for an accurate calibration normal. Nonetheless, at least one accurate distance (e.g. from a scale bar) is needed to fix the scale if absolute measurements are required. On the down side, highly accurate measurements require complicated sensor models and some effects in the image formation process might remain uncorrected. While direct calibration techniques are very popular for light stripe range finders, projection devices that generate 2D patterns have also been modeled as inverse cameras [25,28,29,34].

A range finder can only acquire those parts of an object, which are visible from a given viewpoint. Hence it is necessary to transform data from different viewpoints

into one common coordinate system. Most of the techniques to perform this so-called registration task are more or less variations of the Iterative Closest Point (ICP) algorithm proposed by Besl and McKay [4]. The algorithm can briefly be sketched as follows. Assuming a reasonable good initial registration, the relative orientation between two datasets is iteratively refined by pairing a number of points on one surface with the closest points on the other surface and minimizing the sum of squared distances between the point sets.

Closed form solutions to find the rigid body transformations between two point sets are readily available e.g. [1,17,18,31] and have been compared by Eggert et al [13]. Although [17] considered an isotropic noise model to reflect measurements of unequal quality, none of the methods is capable to handle anisotropic noise. In addition, the methods yield no information about the accuracy of the estimated transformation parameters.

Numerous extensions have been proposed to overcome shortcomings of the original ICP algorithm. A number of heuristics address the problem of partially overlapping surfaces. It is very common to discard correspondences that are too far apart and correspondences that lie on the surface boundary [6,27]. Other authors discard point pairs that are not compatible with the neighboring pairs [11].

All pairwise registration techniques have problems to find a good solution for the case of multiple datasets, since errors in the estimated transformations accumulate if views are added consecutively [9]. For that reason global registration techniques are needed. The solution of Turk and Levoy [27] requires a cylindrical scan that covers a large portion of the object. Linear scans are then registered to this scan using the overlapping portions. Although the method works fine, not all sensors might be able to generate such a cylindrical scan. Blais and Levine [6] define a sequence of transformations between consecutive pairs of images and also between the first and the last image in the sequence. Very fast simulated annealing, a stochastic optimization method, is used to minimize a total cost function. However, the high dimensional minimization problem requires a large processing time. Bergevin et al [2] build a network of transformations between different views. One view defines the reference frame. The correspondences from all possible pairings are used to simultaneously compute the transformations for all views at each iteration. Because of a possible accumulation of registration errors, care has to be taken that the network topology minimizes the lengths of the paths between the nodes. The solution of Pulli [22] enforces constraints from pairwise registration in the global registration step. The method is particularly suited to register large data sets. Since only the constraints are used in global registration there is no need to keep the entire data set in memory, but good pairwise alignments are required. Stoddart and Hilton [24] and Eggert et al

[12] independently followed a completely different approach. They perform a force-based optimization by simulating the interconnection of the data sets with springs between corresponding points and then solve the equation system of the resulting dynamic system.

Only very few registration algorithms have addressed the issue of varying or anisotropic noise. Turk and Levoy [27] take advantage of the optional weighting term in [17]. They assign a confidence value to each point, which is computed as the dot product between the local surface normal and the line of sight of the sensor. A complete framework to describe and treat uncertainty in point set registration has been developed by Pennec and Thirion [20]. They use extended Kalman filtering to estimate the parameters of a rigid body transformation and the parameters covariance matrix. However, the method does not solve the global registration problem. Stoddart et al [24] extended this framework to the problem of surface registration. Pito [21] addressed the problem of insufficient shape information. He performed a qualitative analysis of geometric constraints with respect to rotation and translation and introduced a mechanical registration aid, on which he places the object.

Williams and Bennamoun [33] recently described a global method for point set registration considering a three dimensional Gaussian error model. They also applied a robust (least median of squares) estimation technique but did not address the problem of surface registration. The results were demonstrated using rather small sets of points (10 to 40 points) but with a significant level of outliers.

2 Data Acquisition

2.1 Physical Setup

Our measurement system consists of a commercial stripe projector (ABW LCD 640 Cross, $90\ \mu\text{m}$ line width at 640×640 lines [35]), one or more monochrome cameras (Basler A113 with $2/3''$ imagers, $6.7\ \mu\text{m}$ pixel size at 1296×1024 pixels and $12\ \text{mm}$ Schneider-Kreuznach lenses) and a 3-axis positioning device to place the object or the calibration plate in front of the sensor. The cameras and the projector are mounted on a stable aluminum profile. A PC is used to control the system and process the data. The patterns are generated by switching lines on a two-dimensional LCD illuminated from behind. This type of projector has the advantage that there are no moving parts involved. While normal LCD projectors use two glass plates with conducting stripes aligned precisely, a cross-pattern projector has one of the glass plates turned by 90 degrees. Since all stripes can be switched individually, arbitrary horizontal and vertical stripe patterns can be generated (albeit no arbitrary 2D patterns

can be generated, since the 2D pattern always results from a XOR of the two line patterns).



Figure 1. Physical setup of the measurement system.

2.2 System Calibration

Although calibration is a well-known problem in computer vision and photogrammetry, its importance is often underestimated. In our opinion, system calibration is the limiting factor for the accuracy of most 3D measurement systems.

The calibration method also determines, the way 3D object coordinates are computed. Since we are interested in the covariance matrices of the measured points, too, the black box approach of direct calibration techniques is not appropriate. Consequently, we use a model-based photogrammetric technique to solve for the parameters describing the image formation process. Since the projector is able to generate horizontal and vertical patterns, it can be modeled and calibrated like an inverse camera using a planar test field and a convergent setup.

Our test field consists of an aluminum plate, on which we fixed a sheet of self-adhesive paper showing white dots on a black background. Five of those targets are surrounded by white rings. These rings allow determining the orientation of the test field. In the next step all visible target points are measured and identified fully automatically. Image coordinates for the camera are obtained by computing the weighted centroid. Corresponding projector coordinates are then computed with sub-pixel accuracy by a sampling at the centroid positions. A typical calibration sequence consists of eight views, where the orientation of the calibration plate is changed between different views. The parameters are estimated using the “Australis” software package from the Department of Geomatics of the University of Melbourne.

We use a camera model with 10 parameters, namely the focal length c , the principal point offsets Δx and Δy , K_1 , K_2 and K_3 for radial symmetric distortion, P_1 , P_2 for decentering distortion and B_1 and B_2 for scale and shear [15].

The calibration parameters are introduced to form the well-known extended collinearity model:

$$\begin{aligned} x - x_0 + \Delta x &= -c \frac{R_1}{R_3} \\ y - y_0 + \Delta y &= -c \frac{R_2}{R_3} \end{aligned} \quad (1)$$

where

$$\begin{bmatrix} R_1 \\ R_2 \\ R_3 \end{bmatrix} = R \begin{bmatrix} X - X^0 \\ Y - Y^0 \\ Z - Z^0 \end{bmatrix} \quad (2)$$

These equations describe the perspective transformation between the object space (object point X, Y, Z and perspective center X^0, Y^0, Z^0 with rotation matrix \mathbf{R}) and the image space (image point x, y), where the coefficients Δx and Δy contain the distortion parameters.

The results of the calibration process are the intrinsic and extrinsic parameters of the projector and all cameras in a common coordinate frame.

2.3 Solving the Correspondence Problem

The correspondence problem can be stated as follows. Given a token in one image, find the corresponding tokens in all other images. Once the correspondence problem is solved, the computation of object coordinates is straightforward.

In a previous publication [16] we have proposed a new pattern design, together with a new evaluation method. The so-called line shift pattern consists of a Gray code sequence, followed by a sequence of parallel lines, achieved by illuminating each n^{th} projector line. For our system, we have chosen $n = 6$.

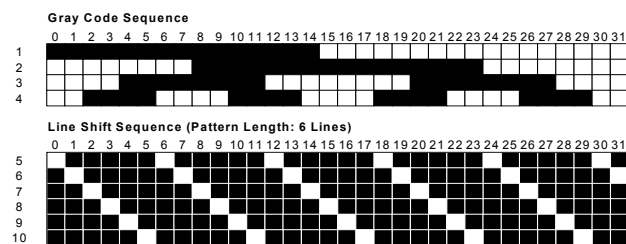


Figure 2. Gray code sequence (top) and line shift sequence (bottom) for a 32 line sensor.

The evaluation of the line shift images is performed similar to the evaluation of images obtained with a light stripe range finder, but in a highly parallel manner. Six images for the x and six images for the y coordinates are needed to exploit the whole resolution of the projector (plus 20 Gray code images for ambiguity resolution).

The line centers are detected with sub-pixel accuracy using a peak detector proposed by Blais and Rioux [5]. The detector performs a convolution of the grayvalue

image with a fourth or eighth order linear filter (derivative operator). It then determines the sub-pixel position of the zero crossing in the convolved image. The Gray code sequence is used to resolve ambiguities and determine uniquely the projector line number. An oversampling technique makes ambiguity resolution more robust

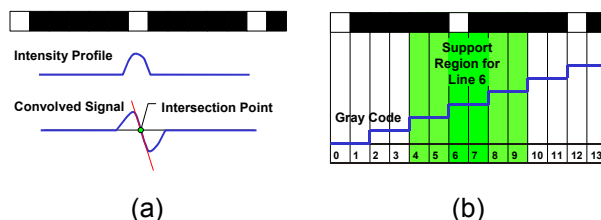


Figure 3. (a) The sub-pixel position of the line center is detected by a linear interpolation of the zero crossing in the convolved line shift image. (b) The distance between consecutive lines in one image is three times the resolution of the Gray code. The oversampling is used to establish support regions during the labeling process, yielding a more robust solution.

In the next step the lines joining the detected stripe centers are intersected to obtain sub-pixel camera coordinates for each projector coordinate.

The transition from the camera domain to the projector domain is particular for the new method. Performing the same steps for an arbitrary number of cameras, immediately gives us not only the correspondences between image points of a single camera/projector combination but also corresponding points between any of the cameras linked by a common projector.

We have also adapted spacetime analysis to work with our system using the line shift sequence. Because the evaluation is faster, it is the method of choice if only one camera is used.

2.4 Object Point Coordinates

Object point coordinates are computed by iterative non-linear least squares adjustment using equations (1) and (2). The solution is found by inverting a 3×3 matrix, which afterwards contains the covariance information. Points that exhibit large residuals, as well as points seen at a steep angle are removed.

Accuracy and reliability can be significantly improved if image data from multiple cameras is available, all sharing the same projector. Because line shift processing directly links projector lines to camera coordinates, corresponding pairs of image points between different cameras can be found easily. Each pair contributes four observations to solve for the three unknown object point coordinates. It is obvious, that a large number of

observations, corresponding to a high redundancy, yield more accurate results.

The data, obtained by multiple cameras, is also used to enforce explicit consistency tests. Specular reflections, as they are likely to occur on the surface of machined metal parts, cause spurious 3D point measurements. The consistency tests are based on the observation, that specular reflections are viewpoint dependent. If the cameras view the object from different angles we can compute the deviation between object points, computed from different pairings of image points. This allows us to discard inconsistent measurements.

The points and their associated covariance matrices are stored in a multi-dimensional image array. It is remarkable that the image, containing the covariance information for the z coordinates usually looks like an embossed image of the object under consideration, because mixed-pixel effects cause larger errors near surface discontinuities.

2.5 Mesh Construction

We use triangular meshes in the further processing steps. Consequently, we have to convert the coordinate arrays into mesh representation. Besides the geometric position, additional information like the components of the covariance matrix and surface intensity information is stored as vertex attributes. Special care has to be taken to avoid the generation of incorrect topology in the presence of surface discontinuities. Our mesh generation algorithm discards triangles if the length of any edge exceeds a distance threshold. We have made good experience using a distance threshold of two to four times the sampling distance. The magnitude of steps in either coordinate direction can be limited, too. The mesh generation algorithm is very similar to the one described in [27].

3 Registration and Model Validation

Registration is required for two purposes within our processing chain. First, measurements from different viewpoints need to be transformed into one common coordinate frame. In general, multiple datasets are concerned, requiring a multi-view registration technique to find a globally optimal solution. Second, the reconstructed model needs to be aligned with its CAD description in order to compute the deviation between the two surfaces. In this case, only two surfaces are concerned and a pairwise registration procedure is appropriate.

We have developed a pairwise and a global registration algorithm. Both algorithms are modifications of the iterative closest point (ICP) algorithm [4]. As in most registration algorithms, the problem of finding a transformation between surfaces is reduced to finding a rigid body transformation that minimizes the least-

squared distance between corresponding point pairs. Unlike most other methods, we use an iterative solution to incorporate anisotropic noise in pose estimation.

3.1 Pose Estimation

Let S be a set of n points $\mathbf{s}_i \in \mathbb{R}^3$, given in the source coordinate frame and D be the set of corresponding points $\mathbf{d}_i \in \mathbb{R}^3$ given in the destination coordinate frame with covariance matrices $\Sigma_{\mathbf{s}_i}$ and $\Sigma_{\mathbf{d}_i}$ respectively. Let $T(\mathbf{q}, \mathbf{t}) = T(\mathbf{R}(\mathbf{q}), \mathbf{t})$ be a rigid body transformation with rotation matrix $\mathbf{R} \in \mathbb{R}^{3 \times 3} \mid \mathbf{R}^T \mathbf{R} = \mathbf{I}_3$ and translation vector $\mathbf{t} \in \mathbb{R}^3$. $\mathbf{R}(\mathbf{q})$ is parameterized using the unit quaternion

$$\mathbf{q} = [q_0 \ q_1 \ q_2 \ q_3]^T \mid q_0 \geq 0 \wedge q_0^2 + q_1^2 + q_2^2 + q_3^2 = 1 .$$

The residuals between the transformed source point $\mathbf{s}'_i = T(\mathbf{q}, \mathbf{t})\mathbf{s}_i$ and the destination point \mathbf{d}_i are defined as

$$\mathbf{v}_i = \mathbf{d}_i - T(\mathbf{q}, \mathbf{t})\mathbf{s}_i = \mathbf{d}_i - \mathbf{R}(\mathbf{q})\mathbf{s}_i + \mathbf{t} \quad (3)$$

It is the goal of pose estimation to find the parameters \mathbf{q} and \mathbf{t} such that the covariance weighted least-squares objective function

$$V = \sum_{i=1}^n \mathbf{v}_i^T W_i \mathbf{v}_i \quad (4)$$

with $W_i = \Sigma_i^{-1}$ is minimized. Assuming the points \mathbf{s}_i and \mathbf{d}_i to be independent, the covariance Matrix Σ_i is computed

$$\Sigma_i = \Sigma_{\mathbf{d}_i} + \mathbf{R} \Sigma_{\mathbf{s}_i} \mathbf{R}^T \quad (5)$$

We use a modified version of the iterative non-linear least squares solution described in [32]. They derive a simple form for the Jacobian of rotation with respect to quaternions when evaluated at the identity quaternion \mathbf{q}_I . In fact, only three rotation parameters (the vector part $[q_1 \ q_2 \ q_3]^T$ of the quaternion) are estimated and used to incrementally update the quaternion. As [32] do not consider the covariance of the estimated parameters, we extended their solution to yield the covariance matrix of all seven transformation parameters (of which only six parameters are independent). The method usually requires one to five iterations and performs excellent in practice.

3.2 Corresponding Point Search

Let M_D be a triangular mesh and Ω_{M_D} denote its boundary. We can define a corresponding point operator $C(M_D, \mathbf{s}, \mathbf{n}_s, t_d, t_a)$ which returns a pair $\langle \mathbf{d}, \Sigma_d \rangle$ if a corresponding point is found or void if no such point exists, where \mathbf{s} is a source point and \mathbf{n}_s its associated surface normal, t_d a distance threshold, t_a an angular

threshold, \mathbf{d} the position of the corresponding point and $\Sigma_{\mathbf{d}}$ its covariance matrix.

A corresponding point \mathbf{d} is defined as the point on the mesh $M_D \setminus \Omega_{M_D}$ that is closest to the given point \mathbf{s} and satisfies the following conditions:

$$\|\mathbf{s} - \mathbf{d}\| < t_d \quad (6)$$

and

$$\mathbf{n}_{\mathbf{s}} \cdot \mathbf{n}_{\mathbf{d}} > t_a \quad (7)$$

where $\mathbf{n}_{\mathbf{d}}$ is the surface normal of M_D at point \mathbf{d} .

The imposed constraints allow for the registration of partially overlapping surfaces. For the most part, the constraints are the same as in [27]. We discard correspondences where either point lies on the mesh boundary and points that are too far apart. In addition, we require the normal of both points to have similar orientation. The last condition prevents from connecting different sides of thin surfaces. It is important to note that the corresponding point \mathbf{d} is defined to lie anywhere on the C^0 continuous surface M_D and is not necessarily a vertex of M_D , yielding higher accuracy.

The corresponding point is located either within or on an edge of a triangle $T = \{\mathbf{d}_i, \mathbf{d}_j, \mathbf{d}_k\} \in M_D$. Its covariance matrix $\Sigma_{\mathbf{d}}$ is computed as

$$\Sigma_{\mathbf{d}} = \alpha^2 \Sigma_{\mathbf{d}_i} + \beta^2 \Sigma_{\mathbf{d}_j} + \gamma^2 \Sigma_{\mathbf{d}_k} \quad (8)$$

where α, β, γ are the barycentric coordinates of the point \mathbf{d} with respect to the triangle T .

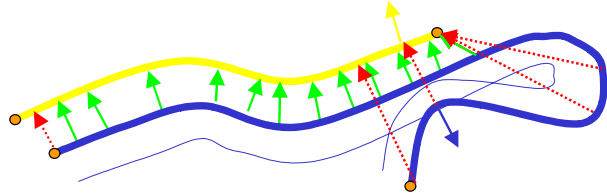


Figure 4. Valid correspondences (green/light grey) and correspondences that have been rejected by the described criteria (red/dark grey).

A naïve implementation would require distance computations to all triangles, edges and vertices of M_D . As this cannot be tolerated for real-world applications, we improve efficiency by using a more sophisticated closest point search. A sparse grid structure is employed to access the relevant triangles in almost constant time.

3.3 Pairwise Registration

Our pairwise registration algorithm aligns the source surface M_S with the destination surface M_D , where M_S

and M_D are triangular meshes with boundaries Ω_{M_S} and Ω_{M_D} . The algorithm performs the following steps:

1. Preprocessing
 - Build the sparse grid structure for the closest point search.
 - Define a set of points $C \in \Omega_{M_S} \setminus \Omega_{M_D}$ called control points on M_S e.g. by using each n^{th} point.
2. Closest Point Search. Find the sets of corresponding points S and D and their covariance matrices, with $S = \{\mathbf{s}_i\}, D = \{\mathbf{d}_i\} \mid S \subset C \wedge \mathbf{d}_i = C(\mathbf{s}_i, \mathbf{n}_{\mathbf{s}_i}, t_d, t_a)$.
3. Pose Estimation. Find the rigid body transformation T that minimizes (4).
4. Apply transformation T to M_S .
5. Terminate the iteration if the change in the parameters falls below a preset threshold or repeat steps 2-5.

The algorithm can register partially overlapping surfaces (due to the definition of the corresponding point operator) using an anisotropic gaussian error model. In addition, the covariance matrix of the transformation parameters is estimated to measure transformation uncertainty.

Pito [21] performed a qualitative analysis on how constraints from surface geometry affect uncertainty in the registration parameters. This work was the motivation to quantitatively address this problem in our algorithm.

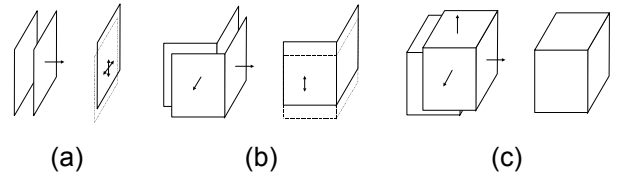


Figure 5. Constraints on registration due to surface geometry. (a) Unconstrained in two directions. (b) Unconstrained in one direction. (c) Fully constrained (adapted from [21]).

In Figure 5, case (a) registration is constrained in direction of the plane normal, but it is not constrained in any orthogonal direction. The reason is, that the established point correspondences carry only information in direction of the line connecting them.

This finding can be incorporated in the pose estimation algorithm by using a modified weight matrix. With

$$\mathbf{v}_i^0 = \frac{\mathbf{d}_i - \mathbf{s}_i}{\|\mathbf{d}_i - \mathbf{s}_i\|} \quad (9)$$

the variance in direction of \mathbf{v}_i^0 can be computed from (5)

$$\sigma_{\mathbf{v}_i}^2 = \mathbf{v}_i^{0T} \Sigma_i \mathbf{v}_i^0 \quad (10)$$

The new weight matrix must reflect the fact, that information is only available in one direction leading to a weight matrix of rank 1

$$\mathbf{W}'_i = \frac{1}{\sigma_0^2} \mathbf{v} \mathbf{v}_i^T = \frac{1}{\sigma_0^2} \begin{bmatrix} v_x^2 & v_x v_y & v_x v_z \\ v_x v_y & v_y^2 & v_y v_z \\ v_x v_z & v_y v_z & v_z^2 \end{bmatrix} \quad (11)$$

Replacing \mathbf{W}_i by \mathbf{W}'_i in equation (4) has two advantages:

1. We achieve a tremendous speed up in convergence (for some surfaces more than factor 50 compared to the previous solution), since the two surfaces are no longer stucked together by apparent observations perpendicular to \mathbf{v}_i .
2. We get a clear diagnosis how well the surface information constraints registration.

Although the solutions have been derived independently and differ in the way the parameters are estimated, for the case of isotropic noise our method yields a similar objective function as was used in [24]. They have also reported a significant reduction in the number of iterations.

3.4 Multi-View Registration

Given a set of n triangular meshes M_{S_i} , our multi-view registration algorithm simultaneously aligns the overlapping parts of all n surfaces. It can be considered as a generalization of the ICP algorithm to the case of multiple surfaces. The idea is as simple as effective: starting from a reasonably good initial registration, we iteratively refine the position of so-called tie points \mathbf{t}_j by computing the weighted average of the corresponding points on all surfaces, which are found using $\mathbf{s}_{ij} C(M_{S_i}, \mathbf{t}_j, \mathbf{n}_{\mathbf{t}_j}, t_d, t_a)$ and the weight matrix $\Sigma'_{s_{ij}}$, which also considers uncertainty in the transformation parameters, where J_{T_i} is the Jacobian of the transformation with respect to the parameters \mathbf{q} and \mathbf{t}

$$\Sigma'_{s_{ij}} = \mathbf{R}_i \Sigma_{s_{ij}} \mathbf{R}_i^T + J_{T_i}(\mathbf{s}_{ij}) \Sigma_{T_i} J_{T_i}(\mathbf{s}_{ij})^T \quad (12)$$

We can then estimate for every surface M_{S_i} the rigid body transformation T_i that minimizes the sum of squared distances to all tie points linked to that surface. The poses of all surfaces are updated and we can start the next iteration until the change in the parameters falls below a preset threshold. Since we iteratively refine the mean position of the tie-points, we call the algorithm *iterative mean point algorithm* (IMP). The steps are:

1. Preprocessing
 - Build the sparse grid structures for the closest point search.

- Find a set of tie points TP by regularly sampling the volume within the combined bounding box of all surfaces. A tie point is created if corresponding points on at least two surfaces are found, using a larger distance threshold $t_{d_{init}}$. Each tie point stores the indices of all surfaces it is initially linked to. Only these surfaces have to be considered for searching corresponding points in later steps of the algorithm.

2. Closest Point Search. Find sets of tie points TP_i , corresponding points S_i and their covariance matrices considering only the relevant surfaces.
$$TP_i = \{\mathbf{t}_i\}, S_i = \{\mathbf{s}_{ij}\} | s_{ij} = C(M_{S_i}, \mathbf{t}_j, \mathbf{n}_{\mathbf{t}_j}, t_{d_{init}}, t_a)$$
3. Mean Point Estimation. Find the mean position $\bar{\mathbf{t}}_j$ of all tie points using (12).
4. Pose Estimation. Find the n rigid body transformation T_i that minimize (4) using all the concepts from pairwise registration and the covariance matrix of the mean points $\bar{\mathbf{t}}_j$.
5. Apply the transformation T_i to the surfaces M_{S_i} .
6. Terminate the iteration if the change in the parameters falls below a preset threshold or repeat steps 2-6.

Like the original ICP algorithm, the new method is general in the sense, that it is independent from surface representation as long as a meaningful corresponding point operator could be defined. The generalization to higher dimensions is straightforward. Since the closest point search could be performed independently for all surfaces, the method is ideally suited for a parallel implementation.

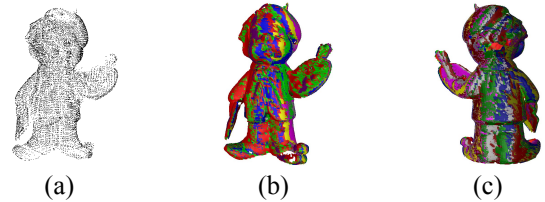


Figure 6. (a) Initial set of tie points. (b),(c) Results of the multiview registration process. The errors are evenly distributed.

3.5 Surface Validation

Surface validation is the task of determining if a measured object is compatible with its CAD model. For this purpose, the sensed dataset is registered with its CAD description. If \mathbf{s}_i denotes a measured point and \mathbf{d}_i denotes its corresponding point on the model, we compute the distance $dev_i = \|\mathbf{d}_i - \mathbf{s}_i\|$ between the two points and compare it to an application dependent threshold t_{dev} .

The uncertainty in the position \mathbf{s}_i is defined by the point's covariance matrix $\Sigma_{\mathbf{s}_i}$, which is computed according to equation (12). From equation (10), we can compute the standard deviation σ_{dev_i} of dev_i . The possible outcomes of the test are:

1. $dev_i - t_{dev} > c\sigma_{dev_i}$ Incompatible.
2. $t_{dev} - c\sigma_{dev_i} < dev_i$ Possibly incompatible.
3. $t_{dev} - c\sigma_{dev_i} > dev_i$ Compatible.

Where c is a constant to control the level of significance α for our test (usually $c = 3$ corresponding to $\alpha \approx 99\%$).

4 Conclusions

A complete processing chain for the acquisition, registration and validation of surfaces incorporating statistical error models has been presented.

We adapted photogrammetric techniques for reliable data acquisition using a structured light system and to provide with point covariance information.

We have proposed and implemented an improved pairwise registration technique and a new multi view-registration algorithm, called iterative mean point algorithm (IMP). Both algorithms achieve higher accuracy and a significant reduction of iterations by using a weighted pose estimation reflecting uncertainty in the observations.

Validation was performed by comparing the measured dataset with its CAD description, considering the uncertainty in the computed deviation.

References

- [1] Arun, K. S., Huang, T. S., and Blostein, S. D., Least-squares fitting of two 3-D point sets, *PAMI*, vol. 9, pp. 698-700, 1987.
- [2] Bergevin, R., Soucy, M., Gagnon, H., and Laurendeau, D., Towards a general multi-view registration technique *IEEE Trans. PAMI*, vol. 18, pp. 540-547, 1996.
- [3] Besl, P. J., Active, optical imaging sensors *Machine Vision and Applications*, vol. 15, pp. 127-152, 1988.
- [4] Besl, P. J. and MacKay, N., A method for registration of 3-D shapes *PAMI*, vol. 14, pp. 239-256, 1992.
- [5] Blais, F. and Rioux, M., Real-time numerical peak detector *Signal Processing*, vol. 11, pp. 145-155, 1986.
- [6] Blais, G. and Levine, M. D., Registering multiview range data to create 3D computer objects *PAMI*, vol. 17, pp. 820-824, 1995.
- [7] Boulanger, P., Moron, V., and Redarce, T., "High-speed and non-contact validation of rapid prototyping parts," *Rapid Product Development Technologies*, pp. 46-60, 1996.
- [8] Brown, D. C., Close-range camera calibration *Photogrammetric Engineering*, vol. 37, pp. 855-866, 1971.
- [9] Chen, Y. and Medioni, G., Object modelling by registration of multiple range images *Image and Vision Computing*, vol. 10, pp. 145-155, 1992.
- [10] Curless, B. and Levoy, M., "Better optical triangulation through spacetime analysis," *Proc. IEEE Int. Conf. on Computer Vision (ICCV)*, pp. 987-994, 1995.
- [11] Dorai, C., Wang, G., Jain, A. K., and Mercer, C., Registration and integration of multiple object views for 3D model construction *PAMI*, vol. 20, pp. 83-89, 1998.
- [12] Eggert, D. W., Fitzgibbon, A. W., and Fisher, R. B., "Simultaneous registration of multiple range views for use in reverse engineering," *Proc. of the 13th Int. Conf. on Patt. Analysis and Machine Intelligence*, pp. 243-247, 1996.
- [13] Eggert, D. W., Lorusso, A., and Fisher, R. B., Estimating 3-D rigid body transformations: a comparison of four major algorithms *Machine Vision and Applications*, vol. 9, pp. 272-290, 1997.
- [14] Everett, H. R., Survey of collision avoidance and ranging sensors for mobile robots *Robotics and Autonomous Systems*, vol. 5, pp. 5-67, 1989.
- [15] Fraser, C. S., Digital camera self-calibration *ISPRS J. of Photogrammetry & Remote Sensing*, vol. 52, pp. 149-159, 1997.
- [16] Gühring, J., Brenner, C., Böhm, J., and Fritsch, D., "Data processing and calibration of a cross-pattern stripe projector," *ISPRS Congress 2000*, 2000.
- [17] Horn, B. K. P., Closed-form solution of absolute orientation using unit quaternions *J. Opt. Soc. Am.*, vol. 4, pp. 629-642, 1987.
- [18] Horn, B. K. P., Hilden, H. M., and Negahdaripour, S., Closed-form solution of absolute orientation using orthonormal matrices *J. Opt. Soc. Am. Ser. A*, vol. 5, pp. 1127-1135, 1988.
- [19] The International Organization for Standardization (ISO), ISO 10360-2: Coordinate metrology - Part 2: Performance assessment of coordinate measuring machines 1997.
- [20] Pennek, X. and Thirion, J.-P., A framework for uncertainty and validation of 3D registration methods based on points and frames *Int. J. of Computer Vision*, vol. 25, pp. 203-229, 1997.
- [21] Pito, R., Automated surface acquisition using range cameras 1996. PhD Thesis, University of Pennsylvania.
- [22] Pulli, K., "Multiview registration for large datasets," *Proc. of 2nd. Int. Conf. on 3D Digital Imaging and Modeling (3DIM'99)*, Ottawa, Canada, pp. 160-168, 1999.
- [23] Rioux, M., "Digital 3-D Imaging: Theory and Applications," *Videometrics III*, 1994.
- [24] Stoddart, A. J., Lemke, S., Hilton, A., and Renn, T., Estimating Pose Uncertainty for Surface Registration *Image and Vision Computing*, vol. 16, pp. 111-120, 1998.
- [25] Trobina, M., ETH-Zürich, BIWI-TR_164, 1995.
- [26] Trucco, E., Fisher, R. B., Fitzgibbon, A. W., and Naidu, D. K., Calibration, data consistency and model acquisition with laser strippers *Int. J. of Computer Integrated Manufacturing*, vol. 11, pp. 293-310, 1998.
- [27] Turk, G. and Levoy, M., "Zippered polygon meshes from range images," *SIGGRAPH '94*, pp. 311-318, 1994.
- [28] Valkenburg, R. J. and McIvor, A. M., "Calibrating a structured light system," Industrial Research Limited, Report 362, 1995.
- [29] Valkenburg, R. J. and McIvor, A. M., "Accurate 3D measurement using a structured light system," Industrial Research Limited, Report 576, 1996.
- [30] VDI/VDE, VDI/VDE 2634 Blatt 2 - Optische 3D-Meßsysteme - Systeme mit flächenhafter Antastung (Entwurf) 2000.
- [31] Walker, M. W., Shao, L., and Volz, R. A., Estimating 3-D location parameters using dual number quaternions *CVGIP: Image Understanding*, vol. 54, pp. 358-367,
- [32] Wheeler, M. D. and Ikeuchi, K., "Iterative estimation of rotation and translation using the quaternion," Technical Report, CMU-CS-95-215, 1995.
- [33] Williams, J. A. and Bennamoun, M., "Multiple view 3D registration using statistical error models," *Vision, Modeling and Visualisation '99*, pp. 83-90, 1999.
- [34] Wiora, G., "High resolution measurement of phase-shift amplitude and numeric object phase calculation," *Vision Geometry IX*, San Diego, 2000.
- [35] Wolf, H., "Vergleichende Betrachtung der verschiedenen strukturierten Lichtquellen von ABW," *Second ABW Workshop*, 1996.